BMC Cancer

RESEARCH

Open Access

Three-dimensional turbo-spin-echo amide proton transfer-weighted and intravoxel incoherent motion imaging mri for triple-negative breast cancer: a comparison with molecular subtypes and histological grades

Nan Zhang[1†], Xiali Shao[1†], Lianyan Xu[1], Wei Zhu[2], Haiyu Wang[2], Rongkui Luo[3], Chun Yang[1], Xiaodan Ye[1], Mengsu Zeng[1], Caizhong Chen[1], Xiuzheng Yue[4], Zhenghong Bi[1,5*†] and Xin Lu[1,5*†]

Abstract

Objective To investigate associations between breast cancer molecular subtype and intravoxel incoherent motion imaging (IVIM) and amide proton transfer-weighted (APTw).

Methods This prospective study involved 264 patients with suspected breast tumors who underwent both breast APTw and IVIM MRI. The maximum diameter of the tumor (Dmax), APT value, apparent diffusion coefficient (ADC), diffusion coefficient (D), pseudo diffusion coefficient (D*), and perfusion fraction (f) values along with histological subtype, grade, and prognostic factors (Ki-67, estrogen receptor (ER), progesterone receptor (PR), human epidermal growth factor receptor-2 (HER-2), were compared. APT values about biological subtypes, Ki-67 labeling index, and nuclear grades (NGs) were further analyzed.

Results A total of 205 participants (mean age, 53 years, range 29–80) were included in the evaluation. The triple-negative breast cancer (TNBC) cancers showed significantly higher D* values than the Luminal B cancers ($P=0.002$), while there was no difference in Dmax, ADC, D, and APT ($P=0.068$,0.318,0.432,0.089). The TN-type cancers showed significantly higher APT values than the HER2-type cancers ($P=0.002$). The area under the curve (AUC) obtained from APTw, IVIM, and Dmax was 0.874. The APT had a moderate positive correlation with the unclear grade ($r=0.473$, $P<0.001$), and the D* had a weak positive correlation with the Ki-67 labeling index($r=0.160$, $P=0.022$).

Conclusion The TN subtype of breast cancer is associated with APT value and D* from IVIM. The APTw may be a promising method for predicting TNBC molecular subtypes.

[†]Xin Lu and Zhenghong Bi contributed equally to this work, they're co-correspondence authors.

[†]Nan Zhang and Xiali Shao contributed equally to this work, they're co-first authors.

*Correspondence:
Zhenghong Bi
bi.zhenghong@zsgmc.sh.cn
Xin Lu
lu.xin@zs-hospital.sh.cn
Full list of author information is available at the end of the article

© The Author(s) 2025. **Open Access** This article is licensed under a Creative Commons Attribution-NonCommercial-NoDerivatives 4.0 International License, which permits any non-commercial use, sharing, distribution and reproduction in any medium or format, as long as you give appropriate credit to the original author(s) and the source, provide a link to the Creative Commons licence, and indicate if you modified the licensed material. You do not have permission under this licence to share adapted material derived from this article or parts of it. The images or other third party material in this article are included in the article's Creative Commons licence, unless indicated otherwise in a credit line to the material. If material is not included in the article's Creative Commons licence and your intended use is not permitted by statutory regulation or exceeds the permitted use, you will need to obtain permission directly from the copyright holder. To view a copy of this licence, visit http://creativecommons.org/licenses/by-nc-nd/4.0/.

Keywords Amide proton transfer weighted, Intravoxel incoherent motion imaging, Biological status, TNBC

Introduction

Breast cancer is the most prevalent malignancy affecting women worldwide [1]. Its heterogeneity arises from a complex interplay of genetic and environmental factors. Based on both molecular and histological markers, breast cancer could be classified into three main categories: hormone receptor-expressing breast cancer (estrogen receptor (ER+) or progesterone receptor (PR+)), breast cancer expressing human epidermal receptor 2 (HER2+), and triple-negative breast cancer (TNBC) (ER−, PR−, HER2−) [2–6]. TNBC, which accounts for 10%−25% of all breast cancers, is defined by the lack of ER, PR, and HER2 expressions [7, 8]. This subtype is notably more aggressive and is associated with a less favorable prognosis. Owing to a lack of well-characterized treatment targets, women with TNBC tumors have fewer treatment options than are available for other breast cancer types and are typically treated with chemotherapy. Relapse is common, usually in the first five years, leading to relatively poor survival outcomes.

Among the differentiation of breast cancer, molecular subtypes is a potentially powerful tool to enable clinicians to better direct and intervene in treatment; genetic analysis presents high hurdles due to cost, specialized equipment, and technical expertise required to process each sample [9]. Therefore, a formal molecular subtype analysis of all breast cancer patients is currently neither practical nor cost-effective. There is great interest in identifying alternative markers for individual molecular subtypes.

There have been many attempts to find a correlation between tumor subtypes and imaging [10].MRI imaging, compared to biopsy as a non-invasive examination method, if related to molecular subtypes, will be used as a potential prognostic indicator since the distinct biological profiles of these subtypes are closely tied to treatment strategies and prognosis [11]. Noninvasive imaging methods that reveal such histologic and molecular characteristic heterogeneity are being developed to guide individualized therapeutic strategies. Among the quantitative MRI methods available, diffusion-weighted imaging (DWI) [12] and chemical exchange saturation transfer (CEST) imaging [13] might help reveal the microstructure and microvasculature within cancer lesions. DWI has been widely used in oncologic imaging, it was shown that ADC values have the highest statistical association with pathological complete response (pCR) prediction in the HER2 enriched subtype [14], Associations between ADC and Ki-67 or tumor grade may be different in other subtypes of BC, such as tubular or medullary carcinomas [15]. Still, studies have shown that ADC cannot predict the hormone receptor status of breast cancer [16]. Intravoxel incoherent motion diffusion-weighted MR imaging (IVIM) has emerged as a promising MRI technique for diagnosing and predicting breast cancers without necessitating contrast agents, which provides quantitative measurements of D (actual diffusion coefficient), D* (pseudo-diffusion coefficient), and f (perfusion fraction), allowing differentiation between lesions of varying aggressive pathological subtypes in breast cancer. D and D* have been shown to indirectly reflect the growth of blood vessels and proteins in cells because of their association with anti-angiogenic [17]. Some researchers [12, 17] have also investigated the association of IVIM parameters with pathological biomarkers. However, no consistent conclusions have been reached regarding the association between IVIM parameters and molecular subtypes.

CEST imaging is an advanced MRI technique that provides information about the microscopic environment of tissues by detecting proton transfer during certain chemical exchange processes, and it can reveal the microscopic structure and microvascular system in cancer lesions [18].The degree of water signal attenuation is proportional to the number of targeted compounds with exchangeable protons; therefore, CEST enables indirect measurement of tissue metabolites, as well as a reflection of the physical and chemical properties of tissues that affect the chemical exchange. In addition, CEST imaging can indirectly reflect the characteristics of the microvascular system by detecting changes in the chemical environment around blood vessels. Changes in metabolites or extracellular pH associated with angiogenesis can be detected by CEST imaging, providing information on the microvascular system [19]. Amide proton transfer-weighted (APTw) MR imaging, as a kind of CEST technology targeting amide protons (resonating at 3.5 ppm downfield from water), reflects the concentration of exchangeable amide protons in endogenous mobile proteins and polypeptide molecules within the cytoplasm. This provides an indirect in vivo assessment of changes in protein expression rates and related pathophysiological information in living cells. Breast cancer is a heterogeneous disease and consists of different molecular subtypes with different angiogenetic characteristics and expressions of genes that regulate vascular normalization. Initial work by Dula et al. [20] first established breast APTw imaging with good stability and repeatability, yet with three patients. Some studies have shown that APTw can be used to evaluate neoadjuvant chemotherapy for breast cancer [21]. More recently, our recent study [22] confirmed the reliability and stability of breast 3D APTw were tested with good results at 3 T, and our team found [23] that APTw showed a significant potential in early

prediction for neoadjuvant chemotherapy treatment in breast cancer. However, a few studies have investigated the association of the APT value with pathological biomarkers. An inconsistent correlation of the APT value with the Ki-67 proliferation index and histologic grade was reported. Liu et al. [24] established that the APT value significantly correlated with the Ki-67 index but showed no significant difference in groups of ER, PR, HER-2, and among molecular subtypes. Kamitani et al. [25] reported that TN and high-Ki-67 breast cancers showed high APT values. These discrepant findings leave the value of APT imaging in evaluating breast cancer ambiguous.

This study aimed to compare the roles of IVIM and APTw in TNBC and analyze the correlations between the derived parameters and the prognostic factors of breast cancer to provide new ideas for the diagnosis, treatment, and predictive assessment of breast cancer.

Materials and methods

Patients

The study was approved by the Institutional Review Board with a requirement for informed consent obtained (approve number: B2022-623R). A total of 264 female patients with breast mass lesions at mammography or ultrasonography were selected for breast MR imaging, of whom 59 patients were excluded for the following reasons: 1) Immunohistochemical and pathological findings were missing ($n=10$), 2) Radiotherapy, chemotherapy, puncture biopsy or pre-scan surgery ($n=14$) 3) Poor lesion visibility on APTw imaging due to tumor size less than 1 cm ($n=35$). Finally, 205 patients with breast cancers were prospectively enrolled in the study between September 1, 2022, and Mar 20, 2024(Fig. 1).

MR imaging protocol

All MR examinations were performed with a 3.0 T whole-body MR scanner (Philips Ingenia CX, Philips Healthcare, the Netherlands) with a dedicated seven-channel bilateral phased-array breast coil. APTw images were acquired using a three-dimensional (3D) turbo-spin-echo (TSE) sequence and IVIM in addition to the traditional imaging protocols (T1WI, T2WI, and DCE imaging); For APTw imaging [22], the saturation pulse train with a duration of 2 s was applied with 2-μT B1 amplitude at each of the following six frequencies for the reconstruction of the Z spectrum in each image voxel: ± 2.7 ppm, ± 3.5 ppm, and ± 4.3 ppm, where 0 ppm was defined as the water proton resonance. A reference acquisition was performed with the radio frequency (RF) at − 1,560 ppm. Three acquisitions were repeated at the saturation frequency of + 3.5 ppm with shifted echo times

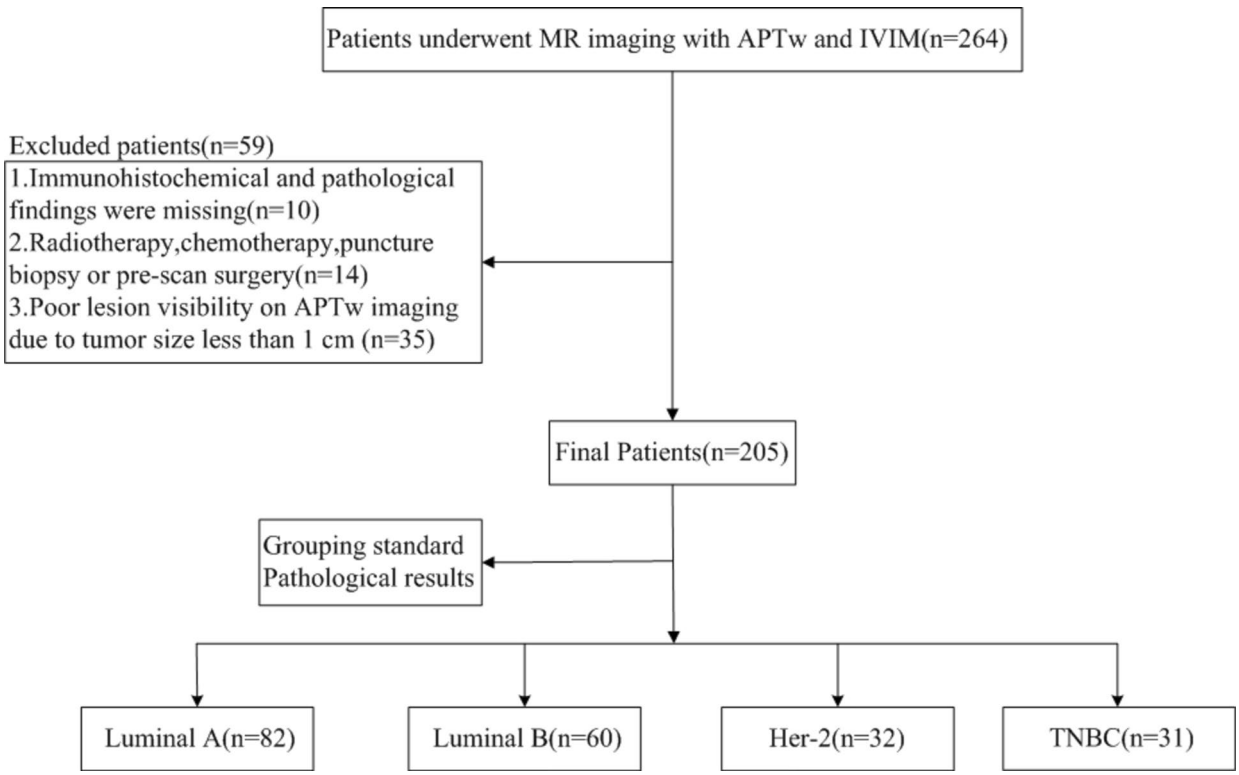

Fig. 1 Flow diagram of the patient selection process

to generate a B0 map for voxel-wise frequency correction to the Z spectra. For reduced influence from B1 field inhomogeneity, unilateral APTw imaging of solely one instead of two breasts was implemented in this study, and to reduce image artifacts induced by the motion of the chest, the prone position of patients was adopted. IVIM (single-shot echo-planar imaging prototype sequence) with spectral attenuated inversion recovery for fat suppression were acquired with the following parameters: b values of 0, 20, 50, 100, 150, 200, 400, 600, 800, 1000, 1500, and 2000s/mm^2. Other imaging parameters are detailed in Table 1. The APTw and IVIM sequences were conducted before the injection of the gadolinium contrast agent (Gadodiamide, Bayer AG). The traditional imaging protocols were prescribed to cover the entire bilateral breast tissue, and the APTw imaging protocol was defined unilaterally to cover the whole tumor based on the images from IVIM.

Image analysis

All APTw and IVIM images were transferred to the IntelliSpace Portal v10.0 workstation (ISP, Philips Healthcare, Best, Netherlands) for image analysis and data measurement. Two breast radiologists performed image analysis (radiologists 1 and 2 were blinded to the final pathological results and other clinical information). The magnetization transfer ratio with asymmetric analysis at + 3.5 ppm (MTRasym(+ 3.5 ppm)) for each image voxel was carried out to generate APTw maps from the raw images in real time on the console with Z-spectrum fitting and B0 correction, as described in the literature [26] where the values in the maps refer to the difference between the signal intensities at ± 3.5 ppm of water proton resonance, as a percentage of the signal intensity when the saturation pulse applied is far off resonance. For each patient, the threshold extraction method for segmentation [27, 28] of the tumors as a whole was carried out according to the following steps independently: 1. the 3D tumor structure was first automatically segmented on DCE images using the MR segmentation software on ISP; 2. manual adjustment was implemented for the tumor segmentation to ensure the inclusion of all tumor; 3. the threshold within the range of 0–1% to 5–8% was manually selected to remove structures of blood vessels and necrosis; 4. the segmentations were copied to APTw and IVIM images for measurement of the mean APT, ADC, D, D* and f values. The APT value was calculated as asymmetry of the traditional magnetization transfer effect at 3.5 ppm on both sides of the water signal:

$$\begin{aligned} \mathrm{APT}\ (\%) &= \mathrm{MTRasym}\ (3.5\ \mathrm{ppm}) \times 100\% \\ &= (S_{sat}(-3.5\mathrm{ppm})/S_0 - S_{sat}(+3.5\mathrm{ppm})/S_0)) \times 100\% \end{aligned} \quad (1)$$

where S_0 is the water signal strength at a saturation frequency of 1540 ppm, and S_{sat} is the water signal strength with a saturation frequency of + 3.5/−3.5 ppm after B0 correction [29].

For DWI, the following formula was used:

$$S_b = S_0 \times exp.(-b \times ADC) \quad (2)$$

where b is the diffusion weight, S_0 refers to the signal intensity (SI) of b = 0 s/mm^2, and S_b refers to the SI at a certain b-value. The ADC is the apparent diffusion

Table 1 Acquisition parameters of all scan sequences

	T1WI	T2WI	IVIM	3D-APT	DCE
TR [ms]	640	1500	6500	6445	4
TE [ms]	8	210	79	7.8	2
FOV [mm^2/mm^3]	240 × 339	240 × 339 × 170	300 × 369	130 × 130 × 49	200 × 315 × 120
Voxel size	1.00 × 1.0	0.80 × 0.90 × 4	1.40 × 1.40	2.03 × 2.00 × 7.00	1.00 × 1.00 × 3.00
Slice thickness[mm]	3	4	3	7	3
Slice Gap	0	−1.5	0	0	−1
Flip angle[°]	90	90	90	90	10
TSE Factor factor	6	92	–	100	–
Acceleration factor	SENSE 3.5	CS2.2	SENSE 4	SENSE 1.6	SENSE2.5
b-value[s/mm2]	–	–	0/20/50/100/150/200/400/600/800/1000/1500/2000	–	–
Fat suppression	–	SPAIR	SPAIR	SPIR	SPAIR
Bandwidth (Hz/pixel)	221.7	1016.3	31.8	702.5	541.1
Saturation pulse/duration	–	–	–	2.0 μT/2 s	–
Scan time (min: sec)	1:55	2:53	7:48	3:58	8:34

CS Compressed sensing, *SENSE* sensitivity encoding, *SPAIR* spectral attenuated inversion recovery, *SPIR* velocity encoding

coefficient [30]. The Mono model was calculated using b-values of 0 and 800 s/mm^2 as utilized.

For IVIM, the raw data were transferred to the ISP for post-processing, and the following formula was used:

$$S_b/S_0 = (1 - f) \times exp.(- bD) + f \times exp.[- bD*] \quad (3)$$

where D represents the true diffusion coefficient, D* represents the pseudo-diffusion coefficient, and f represents the microvascular volume fraction [31]. The IVIM model utilized b-values of 0, 50, 100, 250, 500, 750, and 1000 s/mm^2 due to low b-value region particularly sensitive to tissue vascularity. Some high-b value DWIs were not used in this study. For the two-order single-exponential IVIM model ($IVIM_{mono}$), DWI data fitting was performed using the segmentation constrained algorithm, which sequentially generates IVIM parameters [32]. First, when the b-value > 200 s/mm^2, Eq. (3) can be simplified as mono exponential decay:

$$S_b = S_{int} \times exp.(- bD) \quad (4)$$

where S_{int} is the intercept at b = 0, the D value can be acquired with a least-square fitting by Eq. (4), after which the f value can be estimated through equation $f = (S_0\text{-}S_{int})/S_0$. Finally, the obtained D and f are substituted into Eq. (3), and the non-linear least-square is fitted against all b-values to estimate D*.

Histopathological analysis

All patients underwent mastectomy or breast-conserving surgery. The maximum diameter of the tumor (Dmax) obtained according to the patient's surgical pathological results. The histological type and axillary nodal status were determined based on surgically excised specimens. The estrogen receptor, progesterone receptor, and HER2 statuses were assessed using immunohistochemistry. HER2 staining intensity was scored with ERBB2 0, 1+, 2+, or 3+. Tumors with ERBB2 score of 3+and/or ERBB2 gene amplification confirmed by fluorescence in situ hybridization were regarded as HER2-positive samples. Whether the patient had axillary lymph node metastasis was yes or no. (1) Luminal A type: positive for ER and PR, negative for HER-2 and low expression of Ki-67; (2) Luminal B type can be divided into two subtypes: 1) ER and/or PR positive, HER-2 positive but Ki-67 is not required; 2) ER and/or PR positive, HER-2 negative but Ki-67 high expression; (3) HER-2 overexpression type: ER and PR are negative, HER-2 positive but Ki-67 is not required; (4) Triple-negative breast cancer: ER, PR, and HER-2 are harmful but Ki-67 is not required.

According to the consensus of the St. Gallen Meeting of the International Breast Cancer Expert Group [33], Ki-67 > 20% was defined as high expression, and ≤ 20% was defined as low expression. Ki-67 degradation was determined as Ki-67 degradation from high to low expression. NG was scored for nuclear atypia and mitotic count according to the General Rules for Clinical and Pathological Recording of Breast Cancer [34].

Statistical analyses

Statistical analysis was performed using the SPSS software (version 21, SPSS Inc, Chicago, IL, USA). Intraclass correlation coefficient (ICC) and the Bland–Altman analysis were used to evaluate measurement consistency between the two readers and calculate the 95% limit of agreement (95% LoA). An ICC greater than 0.75 was considered to indicate a good deal. The Kolmogorov–Smirnov test assessed the age, Dmax, APTw value, ADC, D, D*, and f differences between the four groups. The kappa test determined the differences between the four groups in menopausal status and axillary lymph. The parameters with differences were selected for pairwise comparison (TNBC and the other three groups, respectively). Spearman's correlation coefficient was used to analyze the association between the APTw values and Ki-67 expression, nuclear grade, and tumor size. Receiver operating characteristic (ROC) curves were generated to assess the diagnostic performance of MRI parameters and predict subtypes of breast cancers. The Delong test was used to analyze whether there were differences in each parameter's areas under the curve (AUCs).

Results

Clinicopathological data

Two hundred and five patients (mean age 53 years, ranging from 29 to 80 years) were finally included in the study, whose clinical characteristics are summarized in Table 2. The data of the two groups of images were consistent between the two readers (measurements by the two readers are listed in Supplementary material), and results by the senior observer (radiologist 1) were selected for follow-up analysis.

Consistency test

The data measured by the two observers had good consistency. The ICC was 0.885 for D, 0.821 for D*, and 0.867 for f.

Conventional MRI data

Among the 205 patients, 82 breast cancers were Luminal A, 60 breast cancers were Luminal B, 32 breast cancers were HER-2, and 31 breast cancers were TN. These results are shown in Table 3.

Table 2 Patient baseline characteristics

	All ($n=205$)
Mean age (range)	53 (29–88)
Tumor histologic type	
Invasive ductal	203
Invasive lobular	2
Tumor size	
T1	97
T2	92
T3	16
N stage	
N0	105
N1	100
Grade	
1	52
2	75
3	78
Receptor status	
ER positive/PR positive	142
ER negative/PR negative	70
HER2 negative	108
HER2 positive	66
Triple negative	31
Molecular subtype	
Luminal A	82
Luminal B	60
Her-2	32
TN	31

Patient's quantitative MRI Data

APTw and IVIM imaging between molecular subtypes are shown in Fig. 2. Differences for Dmax, APT values, ADC, D, and D* between molecular subtypes were statistically significant, shown in Table 4 and Fig. 3. The TN-type cancers showed no difference between luminal A cancers in Dmax, ADC, D, D* and APT value. ($P=0.515$,0.290, 0.926,0.342,0.839). The TN-type cancers showed significantly higher D* values than the Luminal B cancers ($P=0.002$), with no difference in Dmax, ADC, D, and APT ($P=0.068$,0.318,0.432,0.089). The TN-type cancers showed significantly higher APT values than the HER2-type cancers ($P=0.002$), while there was no difference in Dmax,ADC, D, and D* ($P=0.088$,0.480,0.426,0.923).

Ki67, nuclear grade and tumor size

The D* had a weak positive correlation with the Ki-67 labeling index($r=0.160$, $P=0.022$), with no correlation in APT, ADC D and f ($P=0.463$,0.153,0.644,0.074). The APT had a moderately positive correlation with the nuclear grade ($r=0.473$, $P<0.001$), with no correlation in D*, ADC, D and f ($P=0.423$,0.989,0.574,0.456). The APT, ADC, D, D* and f did not correlate with the tumor size ($P=0.180$,0.147,0.118,0.542,0.564).

Comparison of diagnostic efficacy

The AUC corresponding to APTw and IVIM between the four groups is shown in Table 5. The area under the receiver operating characteristic curve (AUC) of APTw and IVIM for differentiating molecular typing breast cancers is shown in Fig. 4. The combination of APT, IVIM and Dmax values yielded an enhanced diagnostic accuracy (AUC=0.874,0.659,0.852) with a sensitivity of 65.9%,41.0%, 100% and specificity of 100%, 96.8% 71.0% in identifying TNBC and other molecular subtypes. The Delong test showed AUC(APTw+IVIM+Dmax) > AUC(IVIM), AUC(APTw+IVIM+Dmax) > AUC(APTw+IVIM) in Luminal A vs TN; AUC (D+Dmax+APTw) = AUC(D + APTw) > AUC(D),AUC(APTw + IVIM + Dmax) > AUC(IVIM),AUC(APTw + Dmax) > AUC(IVIM

Table 3 Comparison of clinicopathological data

Variable	Total ($n=205$)	LuminalA($n=82$)	Luminal B($n=60$)	HER-2($n=32$)	TN($n=31$)	*p* value
Age						0.575
< 40	37	18	2	8	9	
≥ 40, < 60	106	40	42	10	14	
≥ 60	62	26	14	14	8	
Menstrual status						0.691
yes	169	66	58	20	25	
no	36	16	2	12	6	
Axillary lymph node metastasis						0.870
yes	71	28	18	10	15	
no	134	54	42	22	16	

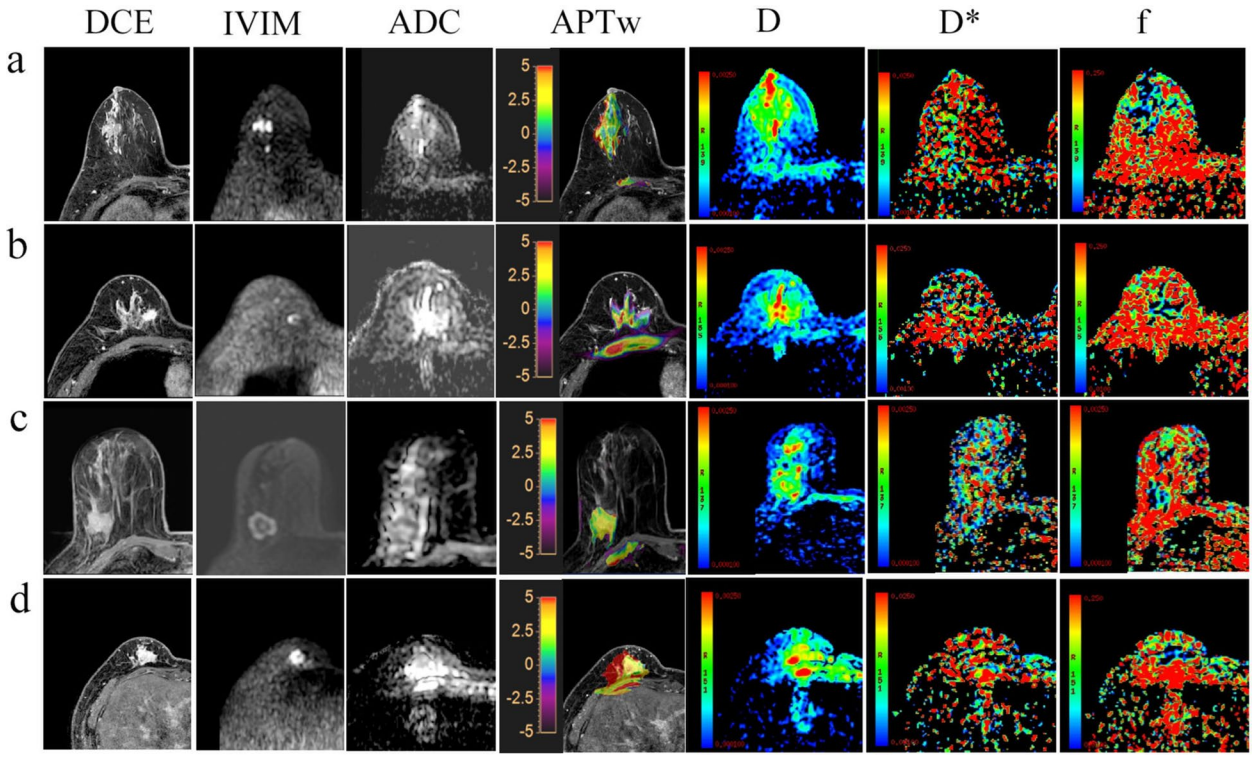

Fig. 2 IVIM parameter maps (ADC,D,D*,f) and APTw superimposed on DCE MRI. Patient 1(**a**) is an invasive ductal breast cancer with luminal A-type. Patient 2(**b**) is an invasive ductal breast cancer with luminal B -type. Patient 3(**c**) is an invasive ductal breast cancer with HER2-type. Patient 4(**d**) is an invasive ductal breast cancer with TN-type

Table 4 Quantitative MRI data

Variable	Luminal A	Luminal B	HER2	TN	*P*
Dmax(mm)	1.70 (1.50,2.13)	2.00 (1.50,2.80)	2.30 (1.80,3.00)	2.30 (2.00,3.00)	< 0.001*
APT(%)	2.30 (1.68,2.71)	2.30 (1.60,2.60)	2.23 (1.90,2.37)	3.20 (2.50,3.70)	< 0.001*
ADC($\times 10^{-3}$mm^2/s)	0.513 (0.57,0.58)	0.49(0.43,0.54)	0.55(0.52,0.57)	0.55 (0.46,0.65)	0.016*
D($\times 10^{-3}$mm^2/s)	0.99 (0.81,1.20)	1.12 (0.93,1.30)	1.22 (1.00,1.30)	1.20 (1.10,1.30)	< 0.001*
D*($\times 10^{-2}$mm^2/s)	2.04 (1.51,2.53)	1.73 (1.58,2.28)	3.40 (1.77,3.60)	2.45 (1.49,3.54)	0.010*
f($\times 10^{-2}$%)	4.82 (1.85,14.85)	5.38 (1.40,11.13)	5.64 (3.45,7.65)	10.80 (3.40,13.20)	0.205

), AUC(APTw + IVIM) > AUC(IVIM) in HER2 vs TN (all $p < 0.05$).

Discussion

Accurate preoperative evaluation of breast cancer subtypes is critical, as distinct biological profiles guide clinical treatments and predict prognosis. We have demonstrated that APTw and IVIM parameters are correlated with a molecular subtype of breast cancer. The TN molecular subtype is associated with APTw. The combination of APT, IVIM and Dmax values yielded an enhanced diagnostic accuracy (AUC = 0.874) with a sensitivity of 65.9% and specificity of 100% in identifying TNBC and Luminal A cancers.

Our results revealed that APT values were higher in TNBC than compared to HER2-enriched cancers, Luminal A and Luminal B type cancers. Liu [24] investigated the four molecular subtypes and showed comparable APT values without statistically significant difference ($P = 0.073$). This result may be because single-slice 2D APT imaging was employed in this study. Such geometric localization may miss the plane with the largest tumor diameter. Our study employed 3D APTw to address intratumoral heterogeneity better. Kamitani [25]

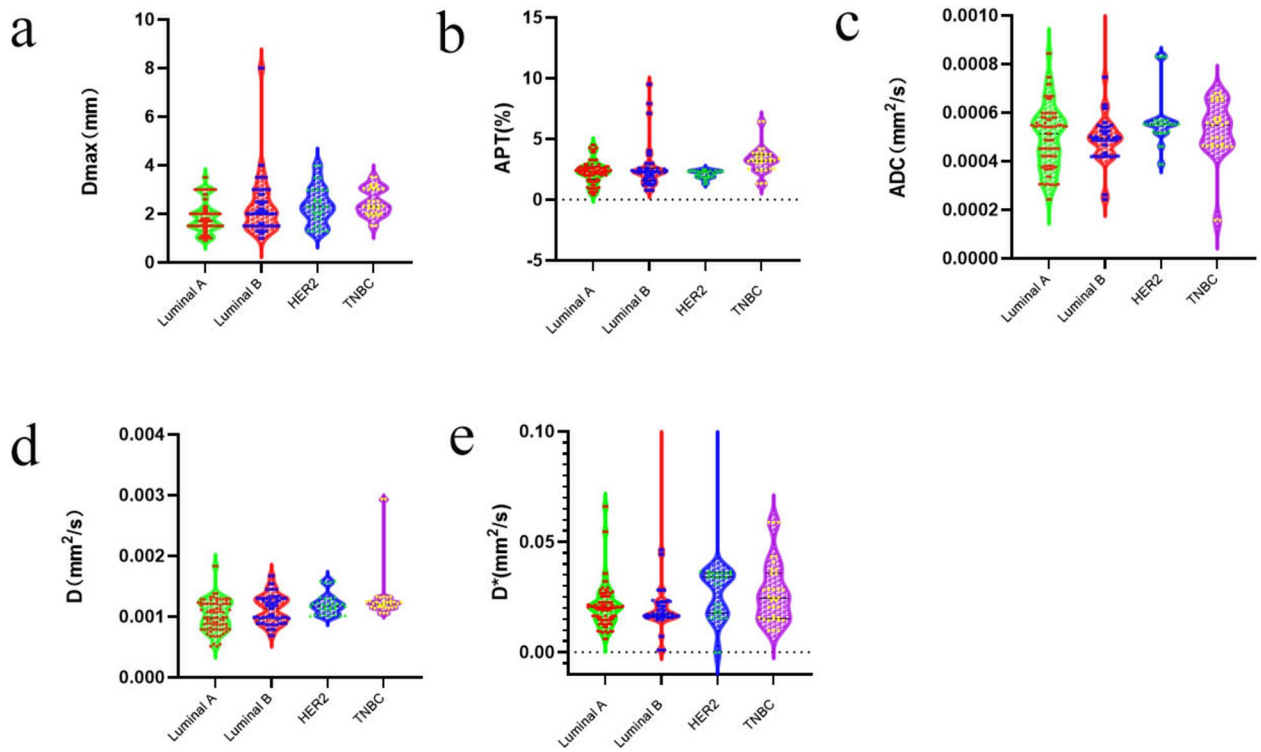

Fig. 3 Violin plots showing Dmax, APT values, ADC,D and D*of different molecular subtypes

Table 5 AUC with sensitivity and specificity of different groups

AUC(Sensitivity(%)/Specificity(%))	Luminal A vs TN	Luminal B vs TN	HER2 vs TN
APT	0.769(85.4/71.0)	0.746(83.6/71)	0.883(93.3/80.6)
ADC	0.602(43.9/93.5)	0.601(77.0/54.8)	0.503(86.7/45.2)
D	0.753(63.4/90.3)	0.625(47.5/100)	0.599(26.7/100)
D*	0.620(73.2/58.1)	0.616(80.3/58.1)	0.566(56.7/71.0)
Dmax	0.775(56.1/93.5)	0.638(59.0/71.0)	0.567(30.0/93.5)
IVIM	0.769(92.7/51.6)	0.599(47.5/100)	0.648(73.3/61.3)
APT&Dmax	0.842(63.4/100)	0.719(86.9/64.5)	0.835(83.3/90.3)
APT&IVIM	0.817(80.5/80.6)	0.617(44.3/96.8)	0.866(93.3/80.6)
APT&IVIM&Dmax	0.874(65.9/100)	0.659(41.0/96.8)	0.852(100/71.0)

used 3D APTw in breast cancer and found that the APT value of TNBC was higher than Luminal type cancers and HER2 cancers, consistent with this study's findings. Patients with TNBC typically have a relatively poorer outcome than those with other breast cancer subtypes owing to inherently aggressive clinical behavior and a lack of recognized molecular targets for therapy [35, 36]. APTw extends the scope of molecular imaging technology to proteins. Liu [24] suggested that APTw may have the potential to assess the aggressiveness of breast cancer. Therefore, it is reasonable that TN cancers showed a high APT value. In addition, large bare nuclei, nuclear atypia, ill-defined borders, necrosis, and lymphocytic cell infiltrate were more common in TNBC as compared to non-TNBC [37]. TNBC has limited treatment options and is usually treated with cytotoxic therapy with poor clinical efficacy [33]. Therefore, it is essential to distinguish TNBC from other subtypes of breast cancers and to find new therapeutic targets for TNBC.

Recent studies of IVIM in breast cancer demonstrated that D, D*, and f values significantly differ from molecular subtypes [38–40]. Our results showed that the D*

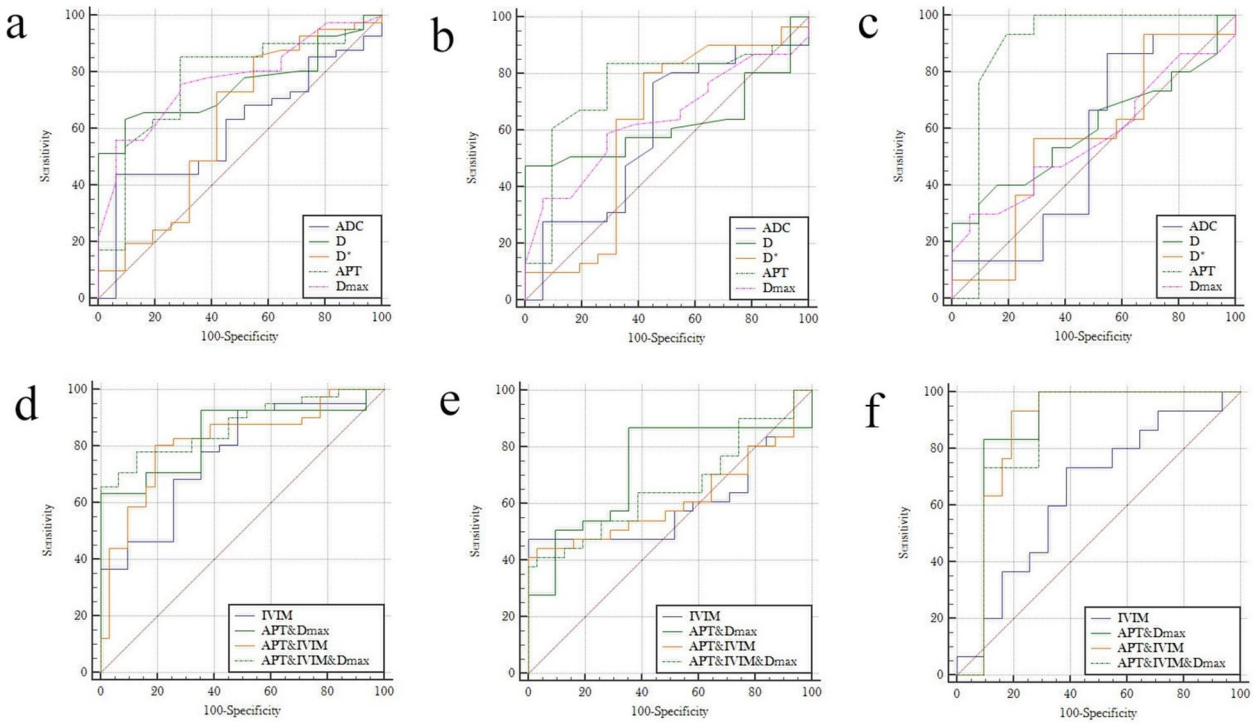

Fig. 4 **a** and (**d**) Receiver operating characteristic curves for individual imaging parameters between Luminal A-type and TNBC; (**b**) and (**e**) Receiver operating characteristic curves for individual imaging parameters between Luminal B-type and TNBC; (**c**) and (**f**) Receiver operating characteristic curves for individual imaging parameters between Luminal A-type and TNBC

values were higher in TNBC than in Luminal B breast cancers, consistent with previous studies. This correlates with the research results of Cho [38], they thought TNBC exhibited increased D* values compared with other subtypes, which suggests that this type of cancer undergoes increased tumor angiogenesis. Our research also found that D* had a weak positive correlation with the Ki-67 labeling index, which supports their view. This is the exact reason for the increase in APT values. In our previous research [22], the APTw value showed a negative correlation with ER expression. This suggests that APTw values could be used as a preliminary indicator of ER expression in breast cancer patients, possibly due to the fact that ER down-regulates vascular endothelial growth factor expression, thereby inhibiting tumor angiogenesis. Similarly, this increase in vascular endothelial growth factor corresponds to an increase in the D* value of IVIM observed in this study. Lee YJ also thought that the D metrics differentiated between ER-positive and -negative groups [41].Our results also showed that ADC cannot predict the hormone receptor status of breast cancer, which is consistent with Meyer H-J [16]. Mami Iima [39] found that the synthetic ADC calculated by using b values of 200 and 1500 tended to decrease in ER-positive tumors compared with ER-negative tumors, and HER2-type tended to show higher synthetic ADC values calculated by using b values of 200 and 1500 among breast tumor statuses. However, this observed trend did not reach the statistical difference after Bonferroni correction, which was consistent with our study. In another research [42], the kurtosis, skewness, uniformity, and entropy values of D values showed a specific predictive ability for the prognostic factors and subtype of breast cancer. Still, there were no significant correlations between D and HER2 expression and lymph node status in this study, which may be related to the variability in HER2 function and small sample size. Lima [39] thought TNBC exhibited increased D values compared to other subtypes. And our IVIM yielded an enhanced diagnostic accuracy (AUC = 0.769) with a sensitivity of 92.7% in identifying TNBC and Luminal A breast cancers, which more sensitive than those reported in previous studies [14, 38].

Interestingly, there was a correlation between Dmax and breast cancer subtypes in our study. Nakashima [43] indicated larger volume increases in TNBC. Given the expected differences in breast cancer growth rates across subtypes, predicting growth rates at diagnosis could facilitate more tailored surgical plans based on patient-specific rates.

Histologic grade, despite tumor size and nodal status, remains prognostically relevant for overall survival. As an independent prognostic factor, breast cancer with a higher histological rate is less differentiated and has a poorer prognosis than breast cancer with a lower histological grade [44]. Most studies have demonstrated the association between APT value and grades [45, 46]. Our analysis suggests a correlation between APT value and grades, but some studies have shown no correlation between them [25]. Several factors could explain this inconsistency, such as the histological type of breast cancer (tumor fever chymosin). Our study also found that APT values were relatively low in stage T1 breast cancer, which we considered related to the relatively slow proliferation of proteins in cells with low stage. More attention has been paid to patients with stage T1, and this finding could help diagnose and treat patients with stage T1 breast cancer [47]. We expect more and more breast cancers to be detected in preinvasive or earlier stages.

The present study suggests that APTw offers an advantage over IVIM in differentiating between TNBC and non-TNBC and prognosis evaluations. Combined IVIM and APTw led to improved diagnostic accuracy (AUC = 0.817). While previous studies [12, 48] demonstrated IVIM diagnostic efficacy across breast cancer subtypes. Also, some previous [25, 45, 46] studies showed that APTw may be related to ER, PR, and HER2 expression. Our study combines the two imaging methods to reveal more possibilities for predicting breast cancer subtypes. Yu [42] combined APTw, IVIM, and DKI to predict the molecular typing of 44 cases of breast cancer (10 cases of TNBC) and found that APT had nothing to do with molecular typing, suggesting that it was caused by breast cancer heterogeneity.

Limitations

This study also has some limitations. (1) We excluded the patients with small lesions because we thought small lesions (< 1cm) impact the accuracy of APTw due to the influence of breast fat and water [49]. (2) The longer scanning time of APT and IVIM, especially the lengthening of the already long routine breast MRI examination time, could compromise patient comfort and trigger motion artifacts. (3) Some high b values were not used in this study and will be analyzed in more depth in subsequent studies.

Conclusion

In conclusion, our study results showed that APTw and IVIM can be used to help identify the breast cancer molecular subtype. APTw is a valuable technique that might be useful to differentiate breast cancer subtypes. A combination of APTw and IVIM imaging may be an effective noninvasive method for clinically assessing TNBC from breast cancer subtypes.

Abbreviations

APTw	Amide proton transfer-weighted
TNBC	Triple-negative breast cancer
TN-type	Triple-negative type
IVIM	Intravoxel incoherent motion imaging;
D	Diffusion coefficient
D*	Pseudo diffusion coefficient
f	Perfusion fraction
ER	Estrogen receptor
PR	Progesterone receptor
HER-2	Human epidermal growth factor receptor-2
NGs	Nuclear grades

Acknowledgements

The authors wish to acknowledge the contribution of the following colleagues for responding to the survey and for providing data: Xin Lu and Zhenghong Bi conceived the study and participated in resources, supervision, review and editing, contributed equally to this work. Mengsu Zeng and Chun Yang participated in study design and coordination. Nan Zhang and Xiali Shao drafted the manuscript, contributed equally to this work. Wei Zhu and Haiyu Wang are in charge of screening clinical patients. Rongkui Luo participated in the pathological workup. Nan Zhang participated in the sequence alignment and scanned. Lianyan Xu collected the clinical materials and radiological data. Xiuzheng Yue Lin help set up the MR protocols and deeply revised the manuscript. All authors read and approved the final manuscript.

Authors' contributions

The authors wish to acknowledge the contribution of the following colleagues for responding to the survey and for providing data: Xin Lu and Zhenghong Bi conceived the study and participated in resources, supervision, review and editing, contributed equally to this work. Mengsu Zeng and Chun Yang participated in study design and coordination. Nan Zhang and Xiali Shao drafted the manuscript, contributed equally to this work. Wei Zhu and Haiyu Wang are in charge of screening clinical patients. Rongkui Luo participated in the pathological workup. Nan Zhang participated in the sequence alignment and scanned. Lianyan Xu collected the clinical materials and radiological data. Xiuzheng Yue Lin help set up the MR protocols and deeply revised the manuscript.

Funding

None.

Data availability

No datasets were generated or analysed during the current study.

Declarations

Ethics approval and consent to participate

The study was approved by Institutional Review Board with requirement for informed consent obtained (approve number: B2022-623R).

Consent for publication

Informed consent was obtained from all individual participants included in the study.

Competing interests

The authors declare no competing interests.

Author details

[1]Department of Radiology, Zhongshan Hospital of Fudan University, No180 Fenglin Road, Xuhui District, Shanghai 200023, People's Republic of China. [2]Department of General Surgery, Zhongshan Hospital of Fudan University, No 180 Fenglin Road, Xuhui District, Shanghai 200023, People's Republic of China. [3]Department of Pathology, Zhongshan Hospital of Fudan University, No180 Fenglin Road, Xuhui District, Shanghai 200023, People's Republic of China. [4]Philips Healthcare, Beijing, China. [5]Shanghai Geriatric Medical Center, No 2560 Chunshen Rd, Shanghai 201104, China.

Received: 7 July 2024 Accepted: 6 March 2025
Published online: 14 March 2025

References

1. Giaquinto AN, Sung H, Miller KD, Kramer JL, Newman LA, Minihan A, Jemal A, Siegel RL. Breast Cancer Statistics, 2022. CA Cancer J Clin. 2022;72(6):524–41.
2. Liedtke C, Mazouni C, Hess KR, Andre F, Tordai A, Mejia JA, Symmans WF, Gonzalez-Angulo AM, Hennessy B, Green M, et al. Response to Neoadjuvant Therapy and Long-Term Survival in Patients With Triple-Negative Breast Cancer. J Clin Oncol. 2023;41(10):1809–15.
3. Lehmann BD, Bauer JA, Chen X, Sanders ME, Chakravarthy AB, Shyr Y, Pietenpol JA. Identification of human triple-negative breast cancer subtypes and preclinical models for selection of targeted therapies. J Clin Invest. 2011;121(7):2750–67.
4. Lao C, Lawrenson R, Edwards M, Campbell I. Treatment and survival of Asian women diagnosed with breast cancer in New Zealand. Breast Cancer Res Treat. 2019;177(2):497–505.
5. Acciavatti RJ, Lee SH, Reig B, Moy L, Conant EF, Kontos D, Moon WK. Beyond Breast Density: Risk Measures for Breast Cancer in Multiple Imaging Modalities. Radiology. 2023;306(3): e222575.
6. Grimm LJ. Breast MRI Provides New Opportunities to Identify Patients at Higher Risk. Radiology. 2023;308(2): e231633.
7. Krishnamurthy S, Poornima R, Challa VR, Goud YG. Triple negative breast cancer - our experience and review. Indian J Surg Oncol. 2012;3(1):12–6.
8. Geyer FC, Rodrigues DN, Weigelt B, Reis-Filho JS. Molecular classification of estrogen receptor-positive/luminal breast cancers. Adv Anat Pathol. 2012;19(1):39–53.
9. Guiu S, Michiels S, André F, Cortes J, Denkert C, Di Leo A, Hennessy BT, Sorlie T, Sotiriou C, Turner N, et al. Molecular subclasses of breast cancer: how do we define them? The IMPAKT 2012 Working Group Statement & #x2020. Ann Oncol. 2012;23(12):2997–3006.
10. Mazurowski MA, Zhang J, Grimm LJ, Yoon SC, Silber JI. Radiogenomic Analysis of Breast Cancer: Luminal B Molecular Subtype Is Associated with Enhancement Dynamics at MR Imaging. 2014;273(2):365–72.
11. Barzaman K, Karami J, Zarei Z, Hosseinzadeh A, Kazemi MH, Moradi-Kalbolandi S, Safari E, Farahmand L. Breast cancer: Biology, biomarkers, and treatments. Int Immunopharmacol. 2020;84: 106535.
12. Uslu H, Onal T, Tosun M, Arslan AS, Ciftci E, Utkan NZ. Intravoxel incoherent motion magnetic resonance imaging for breast cancer: A comparison with molecular subtypes and histological grades. Magn Reson Imaging. 2021;78:35–41.
13. Crescenzi R, Donahue PMC, Mahany H, Lants SK, Donahue MJ. CEST MRI quantification procedures for breast cancer treatment-related lymphedema therapy evaluation. Magn Reson Med. 2020;83(5):1760–73.
14. Surov A, Pech M, Meyer H-J, Bitencourt AGV, Fujimoto H, Baxter GC, Santamaría G, Gilbert FJ, Wienke A. Evaluation of pretreatment ADC values as predictors of treatment response to neoadjuvant chemotherapy in patients with breast cancer - a multicenter study. Cancer Imaging. 2022;22(1):68.
15. Surov A, Clauser P, Chang Y-W, Li L, Martincich L, Partridge SC, Kim JY, Meyer HJ, Wienke A. Can diffusion-weighted imaging predict tumor grade and expression of Ki-67 in breast cancer? A multicenter analysis. Breast Cancer Res. 2018;20(1):58.
16. Meyer H-J, Wienke A, Surov A. Diffusion-Weighted Imaging of Different Breast Cancer Molecular Subtypes: A Systematic Review and Meta-Analysis. Breast Care. 2022;17(1):47–54.
17. Hou W, Xue Y, Qian Y, Pan H, Xu M, Shen Y, Li X, Yu Y. Application of Intravoxel Incoherent Motion Diffusion-Weighted Imaging in Predicting and Monitoring Early Efficacy of Anti-Angiogenic Therapy in the C6 Glioma Rat Model. Front Oncol. 2021;11: 842169.
18. Zhu H, Jones CK, van Zijl PC, Barker PB, Zhou J. Fast 3D chemical exchange saturation transfer (CEST) imaging of the human brain. Magn Reson Med. 2010;64(3):638–44.
19. Chung J, Sun D, Hitchens TK, Modo M, Bandos A, Mettenburg J, Wang P, Jin T. Dual contrast CEST MRI for pH-weighted imaging in stroke. 2024;91(1):357–67.
20. Dula AN, Arlinghaus LR, Dortch RD, Dewey BE, Whisenant JG, Ayers GD, Yankeelov TE, Smith SA. Amide proton transfer imaging of the breast at 3 T: establishing reproducibility and possible feasibility assessing chemotherapy response. Magn Reson Med. 2013;70(1):216–24.
21. Krikken E, Khlebnikov V, Zaiss M, Jibodh RA, van Diest PJ, Luijten PR, Klomp DWJ, van Laarhoven HWM, Wijnen JP. Amide chemical exchange saturation transfer at 7 T: a possible biomarker for detecting early response to neoadjuvant chemotherapy in breast cancer patients. Breast Cancer Res. 2018;20(1):51.
22. Zhang N, Kang J, Wang H, Liu A, Miao Y, Ma X, Song Q, Zhang L, Wang J, Shen Z, et al. Differentiation of fibroadenomas versus malignant breast tumors utilizing three-dimensional amide proton transfer weighted magnetic resonance imaging. Clin Imaging. 2022;81:15–23.
23. Zhang N, Song Q, Liang H, Wang Z, Wu Q, Zhang H, Zhang L, Liu A, Wang H, Wang J, et al. Early prediction of pathological response to neoadjuvant chemotherapy of breast tumors: a comparative study using amide proton transfer-weighted, diffusion weighted and dynamic contrast enhanced MRI. Front Med. 2024;11:1295478.
24. Liu Z, Wen J, Wang M, Ren Y, Yang Q, Qian L, Luo H, Feng S, He C, Liu X, et al. Breast Amide Proton Transfer Imaging at 3 T: Diagnostic Performance and Association With Pathologic Characteristics. J Magn Reson Imaging. 2023;57(3):824–33.
25. Kamitani T, Sagiyama K, Yamasaki Y, Hino T, Wada T, Kubo M, Akiyoshi S, Yamamoto H, Yabuuchi H, Ishigami K. Amide proton transfer (APT) imaging of breast cancers and its correlation with biological status. Clin Imaging. 2023;96:38–43.
26. Togao O, Keupp J, Hiwatashi A, Yamashita K, Kikuchi K, Yoneyama M, Honda H. Amide proton transfer imaging of brain tumors using a self-corrected 3D fast spin-echo dixon method: Comparison With separate B(0) correction. Magn Reson Med. 2017;77(6):2272–9.
27. Zhang N, Zhang H, Gao B, Miao Y, Liu A, Song Q, Lin L, Wang J. 3D Amide Proton Transfer Weighted Brain Tumor Imaging With Compressed SENSE: Effects of Different Acceleration Factors. Front Neurosci. 2022;16(16):876587.
28. Zhang N, Song Q, Liang H, Wang Z, Wu Q, Zhang H, Zhang L, Liu A, Wang H, Wang J, et al. Early prediction of pathological response to neoadjuvant chemotherapy of breast tumors: a comparative study using amide proton transfer-weighted, diffusion weighted and dynamic contrast enhanced MRI. Front Med. 2024;17(11):1295478.
29. Zhou J, Payen J-F, Wilson DA, Traystman RJ, van Zijl PCM. Using the amide proton signals of intracellular proteins and peptides to detect pH effects in MRI. Nat Med. 2003;9(8):1085–90.
30. Jiang JX, Zhao JL, Zhang Q, Qing JF, Zhang SQ, Zhang YM, Wu XH. Endometrial carcinoma: diffusion-weighted imaging diagnostic accuracy and correlation with Ki-67 expression. Clin Radiol. 2018;73(4):413.e411-413.e416.
31. Chevallier O, Zhou N, Cercueil JP, He J, Loffroy R, Wáng YXJ. Comparison of tri-exponential decay versus bi-exponential decay and full fitting versus segmented fitting for modeling liver intravoxel incoherent motion diffusion MRI. NMR in Biomed. 2019;32(11):e4155.
32. Park HJ, Sung YS, Lee SS, Lee Y, Cheong H, Kim YJ. Lee Mg: Intravoxel incoherent motion diffusion-weighted MRI of the abdomen: The effect of fitting algorithms on the accuracy and reliability of the parameters. J Magn Reson Imaging. 2016;45(6):1637–47.
33. Goldhirsch A, Winer EP, Coates AS, Gelber RD, Piccart-Gebhart M, Thurlimann B, Senn HJ. Panel m: Personalizing the treatment of women with early breast cancer: highlights of the St Gallen International Expert Consensus on the Primary Therapy of Early Breast Cancer 2013. Ann Oncol. 2013;24(9):2206–23.
34. Sakamoto G, Inaji H, Akiyama F, Haga S, Hiraoka M, Inai K, Iwase T, Kobayashi S, Sakamoto G, Sano M, et al. General rules for clinical and pathological recording of breast cancer 2005. Breast Cancer. 2005;12(Suppl):S1-27.
35. Malorni L, Shetty PB, De Angelis C, Hilsenbeck S, Rimawi MF, Elledge R, Osborne CK, De Placido S, Arpino G. Clinical and biologic features of triple-negative breast cancers in a large cohort of patients with long-term follow-up. Breast Cancer Res Treat. 2012;136(3):795–804.
36. Maranta AF, Broder S, Fritzsche C, Knauer M, Thurlimann B, Jochum W, Ruhstaller T. Do YOU know the Ki-67 index of your breast cancer patients? Knowledge of your institution's Ki-67 index distribution and its robustness is essential for decision-making in early breast cancer. Breast. 2020;51:120–6.
37. Kala C, Athar M, Kala S, Khan L, Jauhari RK, Satsangi A. Clinical and Cyto-Morphological Characterization of Triple Negative Breast Cancer. J Cytol. 2019;36(2):84–8.
38. Cho GY, Moy L, Kim SG, Baete SH, Moccaldi M, Babb JS, Sodickson DK, Sigmund EE. Evaluation of breast cancer using intravoxel incoherent motion (IVIM) histogram analysis: comparison with malignant status,

histological subtype, and molecular prognostic factors. Eur Radiol. 2016;26(8):2547–58.
39. Iima M, Kataoka M, Kanao S, Onishi N, Kawai M, Ohashi A, Sakaguchi R, Toi M, Togashi K. Intravoxel Incoherent Motion and Quantitative Non-Gaussian Diffusion MR Imaging: Evaluation of the Diagnostic and Prognostic Value of Several Markers of Malignant and Benign Breast Lesions. Radiology. 2018;287(2):432–41.
40. Tsai WC, Chang KM, Kao KJ. Dynamic Contrast Enhanced MRI and Intravoxel Incoherent Motion to Identify Molecular Subtypes of Breast Cancer with Different Vascular Normalization Gene Expression. Korean J Radiol. 2021;22(7):1021–33.
41. Lee YJ, Kim SH, Kang BJ, Kang YJ, Yoo H, Yoo J, Lee J, Son YH, Grimm R. Intravoxel incoherent motion (IVIM)-derived parameters in diffusion-weighted MRI: Associations with prognostic factors in invasive ductal carcinoma. J Magn Reson Imaging. 2016;45(5):1394–406.
42. Yu T, Li L, Shi J, Gong X, Cheng Y, Wang W, Cao Y, Cao M, Jiang F, Wang L, et al. Predicting histopathological types and molecular subtype of breast tumors: A comparative study using amide proton transfer-weighted imaging, intravoxel incoherent motion and diffusion kurtosis imaging. Magn Reson Imaging. 2024;105:37–45.
43. Nakashima K, Uematsu T, Takahashi K, Nishimura S, Tadokoro Y, Hayashi T, Sugino T. Does breast cancer growth rate really depend on tumor subtype? Measurement of tumor doubling time using serial ultrasonography between diagnosis and surgery. Breast Cancer. 2019;26(2):206–14.
44. Schwartz AM, Henson DE, Chen D, Rajamarthandan S. Histologic grade remains a prognostic factor for breast cancer regardless of the number of positive lymph nodes and tumor size: a study of 161 708 cases of breast cancer from the SEER Program. Arch Pathol Lab Med. 2014;138(8):1048–52.
45. Meng N, Wang XJ, Sun J, Huang L, Wang Z, Wang KY, Wang J, Han DM, Wang MY. Comparative Study of Amide Proton Transfer-Weighted Imaging and Intravoxel Incoherent Motion Imaging in Breast Cancer Diagnosis and Evaluation. J Magn Reson Imaging. 2020;52(4):1175–86.
46. Meng N, Wang X, Sun J, Han D, Bai Y, Wei W, Wang Z, Jia F, Wang K, Wang M. A comparative study of the value of amide proton transfer-weighted imaging and diffusion kurtosis imaging in the diagnosis and evaluation of breast cancer. Eur Radiol. 2021;31(3):1707–17.
47. Perez CA. Breast conservation therapy in patients with stage T1–T2 breast cancer: current challenges and opportunities. Am J Clin Oncol. 2010;33(5):500–10.
48. Zhao M, Fu K, Zhang L, Guo W, Wu Q, Bai X, Li Z, Guo Q, Tian J. Intravoxel incoherent motion magnetic resonance imaging for breast cancer: A comparison with benign lesions and evaluation of heterogeneity in different tumor regions with prognostic factors and molecular classification. Oncol Lett. 2018;16(4):5100–12.
49. Zhang S, Keupp J, Wang X, Dimitrov I, Madhuranthakam AJ, Lenkinski RE, Vinogradov E. Z-spectrum appearance and interpretation in the presence of fat: Influence of acquisition parameters. Magn Reson Med. 2018;79(5):2731–7.

Publisher's Note

Springer Nature remains neutral with regard to jurisdictional claims in published maps and institutional affiliations.